Journal of Power Sources 323 (2016) 189–200

Contents lists available at ScienceDirect

Journal of Power Sources

journal homepage: www.elsevier.com/locate/jpowsour

A catalyst layer optimisation approach using electrochemical impedance spectroscopy for PEM fuel cells operated with pyrolysed transition metal-*N*-C catalysts

Daniel Malko [a], Thiago Lopes [b], Edson A. Ticianelli [b], Anthony Kucernak [a, *]

[a] Department of Chemistry, Imperial College London, South Kensington Campus, London, SW7 2AZ, UK
[b] Instituto de Química de São Carlos, São Carlos, 13566-590, Brazil

HIGHLIGHTS

- Study of ionomer/catalyst ratio of three non precious metal catalysts for fuel cells.
- Electrochemical Impedance Spectroscopy highlights key factors influencing performance.
- Performance metrics from EIS guide an iterative approach to maximise performance.
- Simple flow diagram allows rapid determination of optimum ionomer/catalyst ratio.

ARTICLE INFO

Article history:
Received 5 February 2016
Received in revised form
26 April 2016
Accepted 9 May 2016

Keywords:
Nafion content
Ionomer to catalyst ratio
Non-precious metal catalysts
Electrochemical impedance spectroscopy
Oxygen reduction reaction

ABSTRACT

The effect of the ionomer to carbon (I/C) ratio on the performance of single cell polymer electrolyte fuel cells is investigated for three different types of non-precious metal cathodic catalysts. Polarisation curves as well as impedance spectra are recorded at different potentials in the presence of argon or oxygen at the cathode and hydrogen at the anode. It is found that a optimised ionomer content is a key factor for improving the performance of the catalyst. Non-optimal ionomer loading can be assessed by two different factors from the impedance spectra. Hence this observation could be used as a diagnostic element to determine the ideal ionomer content and distribution in newly developed catalyst-electrodes. An electrode morphology based on the presence of inhomogeneous resistance distribution within the porous structure is suggested to explain the observed phenomena. The back-pressure and relative humidity effect on this feature is also investigated and supports the above hypothesis. We give a simple flowchart to aid optimisation of electrodes with the minimum number of trials.

1. Introduction

Commercialisation of low temperature fuel cells requires significant cost reductions [1]. Replacing expensive platinum at the cathode with non-precious metal based catalysts (NPMCs) is a promising option. Numerous different catalysts have recently been developed that are all based on carbon doped with heteroatoms, such as nitrogen, and transition metal centres such as Fe or Co [2]. Although these materials show remarkable activity under fuel cell operating conditions, their intrinsic catalytic activity is still lower than that of Pt [2,3]. Due to the lower price, a higher loading is required to compensate for this drawback. However it is not possible to increase the thickness of the catalyst layer (CL) in the membrane electrode assembly (MEA) beyond a certain value. This is partly because proton resistance (ρ_{H^+}), electronic resistance of the CL (ρ_{el_cath}) and mass transport resistance (ρ_{mt}) become limiting factors as the thickness is increased. This will eventually outweigh the benefit of more catalyst. Therefore the US department of energy (DoE) defined targets (2020) for the volumetric activity of non-precious metal catalysts of >300 A cm^{-3} at 0.8 V cell voltage [4].

It has been shown that the ionomer to carbon (I/C) ratio is a significant performance determining factor, both for Pt based catalysts and for non-precious metal catalysts [5,6]. Moreover for Pt on carbon it has been shown that the optimal ionomer content depends strongly on the microstructure of the carbon support and the

* Corresponding author.
E-mail addresses: d.malko@gmx.de (D. Malko), tlopeschem@gmail.com (T. Lopes), edson@iqsc.usp.br (E.A. Ticianelli), anthony@imperial.ac.uk (A. Kucernak).

http://dx.doi.org/10.1016/j.jpowsour.2016.05.035

influence of the ionomer content on the proton conductivity has also been well investigated [6,7]. The typical I/C ratio for platinum based catalyst layers is between 0.9 and 1.0 [6]. These studies helped to understand the behaviour of the catalyst layer and provided information that led to a significant performance increase in cathodes operated with platinum based catalysts. However, these results cannot be easily translated to cathodes operated on NPMCs. This is firstly because the microstructure and composition of newly developed NPMCs varies widely [3]. Secondly, while the activity of precious metal catalysts is localized on micro- and/or nanoparticles that are attached to the carbon support, the activity in non-precious metal catalysts is believed to be highly dispersed within the structure itself or situated on the opening of micropores [8]. This has tremendous impact on the requirements for proton and gas transport within the catalyst layer.

Much work has been devoted to tune the ionomer content and electrode preparation process for precious metal catalysts in order to facilitate efficient proton and gas transport to the reaction site and water away from the reaction site [9–20]. While a homogeneous ionomer coverage is on the one hand desired for effective proton transport it is on the other hand detrimental for the gaseous reactant transport as it creates a barrier for the reactant to access the active site, resulting in mass transport resistance. Numerous NPMCs have already been reported in fuel cells under different conditions and with various ionomer loadings [21–26]. However to date there is no study that investigates the species transport phenomena present within such catalyst layers.

Here, we employ impedance spectroscopy in combination with a varying ionomer content on three different NPMCs with different activity and microstructure to investigate the impact of the I/C ratio on their performance. Experiments were made in the presence and absence of reactant in order to gain deeper insight into the operation of the fuel cell and to determine whether the ionomer content is too high or too low by EIS. This analysis opens the way to a understanding of the behaviour of non-precious metal catalyst layers, which is fundamental for the further development of alternative oxygen reduction reaction catalysts. Furthermore it helps to develop a simple strategy for the estimation of the optimal I/C ratio for a newly prepared NPMC thus accelerating developments in this field.

2. Experimental

2.1. Catalyst synthesis

The catalyst denoted **FeCo** was synthesized following a published method [27]. In a typical route, 0.5 g of carbon black (Ketjenblack® EC-600JD) was refluxed in 200 mL of a 1.0 mol dm^{-3} HCl solution at 80 °C for 8 h to remove trace metals from the carbon black. Subsequently, this was vacuum filtrated, washed with plenty of ultrapure water (18.2 MΩ cm) and dried at 80 °C for 10 h. 200 mg of this pre-treated carbon black was weighted and dispersed in approximately 70 mL of absolute ethanol in an ultrasonication bath. A separate beaker was used to dissolve, in 30 mL of absolute ethanol (VWR), 0.0058 g of $FeCl_3$ (Sigma-Aldrich), 0.0063 g of $Co(NO_3)_2$ (Sigma-Aldrich) along with 2 mL of *N*-ethylamine (Sigma Aldrich). This solution was added to the carbon black suspension and left to reflux for 8 h at 80 °C in a water bath. Subsequently, the resulting solids were filtered and washed with ultrapure water and dried in an oven at 100 °C for 8 h. The dried powders were heat-treated in a tubular oven at 900 °C under nitrogen atmosphere for 1 h after ramping the temperature from room temperature at 20 °C min^{-1}. Finally, the catalysts were refluxed in 100 mL of 0.5 mol dm^{-3} H_2SO_4 at 80 °C for 24 h to remove soluble metal phases. This suspension was vacuum filtrated and washed with excess ultrapure water and dried at 80 °C for 10 h. The catalyst denoted **Fe-1** was prepared as per another literature method [28]. In a 250 mL round bottom flask, 1 g of 1,5-Diaminonaphthalene (98%, VWR) was dissolved in Ethanol (220 mL, absolute, VWR). A solution of 40 mg $FeCl_2{}^*4H_2O$ (Sigma-Aldrich) dissolved in ethanol (20 mL, absolute, VWR) was added to the solution. After 10 min 1 g $NH_4S_2O_8$ (99.9%, Sigma-Aldrich) was also added. The mixture was stirred for 24 h. The solvent was then removed under reduced pressure and the remaining black powder subjected to heat treatment in the tube furnace to 950 °C at a heating rate of 20 °C/min for 2 h, while supplying a constant stream of inert nitrogen gas (Research Grade, BOC). After cooling down, the resulting black powder was refluxed for 8 h in 0.5 mol dm^{-3} H_2SO_4 to remove residual metal. After drying and second heat treatment at 900 °C for 1 h under N_2 the catalyst was ready to use. The catalyst denoted **Fe-2** was prepared as **Fe-1** with the addition of a 1/1 wt ratio of MgO nanopowder (5 nm, Sigma-Aldrich) to the precursor synthesis, in order to change the microstructure. The MgO template is removed during the acid washing stage after the first heat treatment.

2.2. Rotating disk electrode measurements

For the electrochemical experiments using the Rotating Disk Electrode (Pine Instruments, model AFE6R1AU having a mirror polished glassy carbon as disk and rotator model AFMSRCE), the catalyst was deposited on the glassy carbon disk following a procedure described in the literature [29]. A three compartment electrochemical glass cell was used for the aqueous electrochemical tests; the 0.5 mol dm^{-3} H_2SO_4 electrolyte was prepared from concentrated H_2SO_4 97% Aristar from VWR. The RHE reference electrode (GaskatelHydroFlex) was ionically connected to the main compartment of the electrochemical glass cell via a Luggin-Haber-Capillary. A glassy carbon rod was used as counter electrode and ionically connected to the main compartment of the glass cell through a porous frit. Glassy carbon was used as the counter electrode material instead of Pt or Au in order to avoid contamination with catalytically active precious metals. A potentiostat/galvanostat (Autolab, model PGSTAT20) was used for potential or current control during the electrochemical measurements. Steady state oxygen reduction reaction polarisation curves, performed in O_2 saturated electrolyte solutions were obtained via step potentials of 30 mV with a waiting time of 30 s. Ultrapure gases utilized in this study were Nitrogen and Oxygen (BIP plus-X47S, Air products, 99.9999%).

2.3. Single cell setup and performance evaluations

Membrane Electrode Assemblies (MEA) were prepared according to a method developed by Paganin et al. [30] Briefly, considering the targeted I/C ratio, the desired amount of carbon catalyst was mixed with Nafion™ ionomer solution (Aldrich, 5 wt%) and 1.5 mL of isopropanol. This solution was homogenized in an ultrasound bath for 10 min, followed by complete evaporation of the solvents at room temperature. The dried solids were dispersed in isopropanol and quantitatively deposited on a gas transport medium (Toray paper TGP 60 with microporous layer, Alfa Aesar). As anode electrodes, commercial Johnson Matthey platinum electrodes, at a platinum loading of 0.4 mg_{Pt} cm^{-2} (Alfa Aesar, Johnson Matthey, Hydrogen Reformate/Cathode) were used. The membrane and electrode assemblies (MEAs) were obtained by hot-pressing anode and cathode electrodes on both sides of a pre-treated Nafion™ 115 membrane (H^+, DuPont) at 145 °C and 400 kg cm^{-2}, for 3 min. The thicker Nafion™ 115 membrane was deliberately chosen over the thinner 221 membranes in order to avoid the possibility of any Pt crossover from the anode. Single PEFC tests refer to a 5 cm^2

Table 1
Microporous, external and total surface area (SA) as determined by the BET method and the Broekhoff-DeBoer thickness equation.

Catalyst	Micropore SA/m^2 g^{-1}	Mesopore SA/m^2 g^{-1}	Total SA/m^2 g^{-1}
FeCo	394	395	789
Fe-1	362	116	478
Fe-2	679	570	1249

electrode area and single serpentine flow fields (PEFC hardware from Fuel Cell Technologies, Inc.). During PEFC tests pure hydrogen (White Martins, 99.99%) was used at a flow rate of 160 ccm and pure oxygen (White Martins, 99.99%) at a flow rate of 550 ccm. Both anode and cathode compartments of the cell were pressurized with a backpressure of 2 bar (gauge). PEFCs activation and polarisation curves were performed under galvanostatic mode with a fuel cell test station from Fuel Cell Technologies, Inc. The fuel cell hardware was maintained at a temperature of 80 °C. Different relative humidity values were achieved by adjusting the temperature of the humidification bottles. Moreover the backpressure of the system was corrected to account for the different water partial pressure and to match the back pressure at 100% RH. Before any data collection it was ensured that the cell was stable at the respective current density, with a potential drift below 5 mV/h.

2.4. AC impedance measurements

Electrochemical Impedance spectroscopy (EIS) experiments were carried out from 100 kHz to 0.1 Hz and at 10 points per decade using a potentiostat/galvanostat, Autolab model 302 N. Measurements were carried out in the H_2/O_2 PEMFC working under galvanostatic mode, with the AC current modulation (peak-to-peak) being 5% of the DC current when oxygen was present at the cathode. For measurements in the absence of oxygen, the cathode was purged with argon for 30 min prior to EIS measurement under flowing Ar (550 sccm). For these measurement EIS was conducted potentiostatically at 0.1 V with an AC excitation of 5 mV_{p-p} (i.e. 5% of polarisation). It was ensured that no faradaic current was detected prior to data collection. Linearity of the current/potential response was verified for every measurement. Cells were conditioned at the desired DC current or the desired potential for 60 s prior to EIS experiments. Care was taken to minimize the inductance of the collection leads and cell. Moreover, to ensure a good signal to noise ratio, every data point was collected over 5 integration cycles with an integration time of 0.125 s per cycle. To further ensure validity of the collected data, collection was made from high to low frequency,

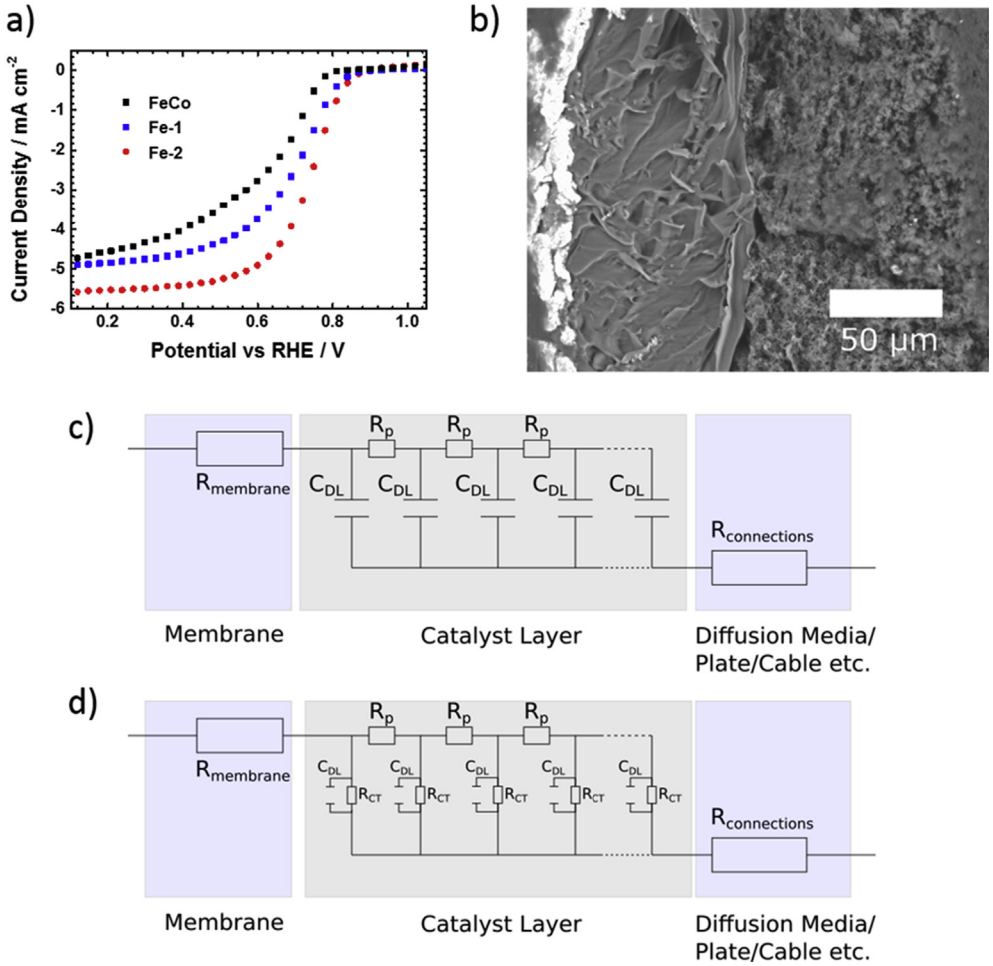

Fig. 1. a) Rotating Disk Electrode (RDE) steady-state polarisation curve for different non-precious metal catalysts. Catalyst loading: 750 µg cm^{-2}, Rotation Rate: 1600 rpm, O_2-saturated 0.5 M H_2SO_4, 30s hold 30 mV step potential. **b)** Representative scanning electron micrograph showing the freeze fractured cross section of a membrane electrode assembly, with the anode catalyst layer/membrane/cathode catalyst layer from left to right. **c)** Transmission line equivalent circuit of the catalyst layer (grey) between the membrane (ionic) and electronic resistive elements in the absence of a faradaic reaction, with the protonic resistance R_p and the double layer capacitance C_{DL}. **d)** Transmission line equivalent circuit in the presence of a faradaic reaction represented by the addition of the charge transfer resistance R_{CT}.

as well as from low to high frequency for selected cells with several hours of operation in between. No significant deviation was detected. All data were checked for Kramers-Kronig conformity according to an improved method developed by Schoenleber et al. [31–33] No drift in the spectra were detected. The correction of the Impedance spectra for high frequency resistance was performed in order to allow a better cross comparison of the catalysts. The correction also reveals the important 45° degree feature in the Bode phase plot. Correction was performed by subtracting the high frequency resistance extracted from the high frequency intercept on the real axis of the Nyquist plot, where the phase angle is zero. The phase angle and modulus were then recalculated with the corrected real part of the impedance and plotted accordingly.

2.5. Scanning electron microscopy

The SEM samples were prepared by freeze fracturing at liquid nitrogen temperature in order to ensure a clean cut. A Hitachi TM3030 operated in secondary electron mode was used for recording the images of the MEA cross section at low magnification. For the high resolution catalyst layer images, a high resolution field emission gun scanning electron microscope (LEO Gemini 1525 FEGSEM) was used.

3. Results and discussion

To characterize the structural differences of the catalysts, the BET surface area was determined by nitrogen adsorption analysis. The isotherms can be found in the Supporting Information. The BET measured micropore, mesopore and total surface areas of the catalyst powders are shown in Table 1. Not only do these catalysts have a different total BET surface area, but also the ratio of macroporous to microporous surface are different.

The Barrett-Joyner-Halenda (BJH) pore size distribution is also qualitatively different for each sample (see Supporting Information S2 and S3). Results in Table 1 show that these catalysts have a different total BET surface areas and different ratios of macroporous to microporous surface. While the templated catalyst Fe-2 has a significantly higher proportion of pores in the 50 Å range, the non-templated catalyst Fe-1 has a significantly lower surface area in this range and exhibits a maximum of pore size distribution in the 100–200 Å range. The Ketjen Black based catalyst (FeCo) on the other hand does not present a distinct maximum in the pore size distribution at these pore size ranges because this maximum is more shifted towards smaller pores. All these structural differences might lead to a different covering and pore filling mechanism of Nafion. Hence the optimal Nafion content might not necessarily be easily correlated to the BET surface area.

The electrochemical performance of the differently prepared

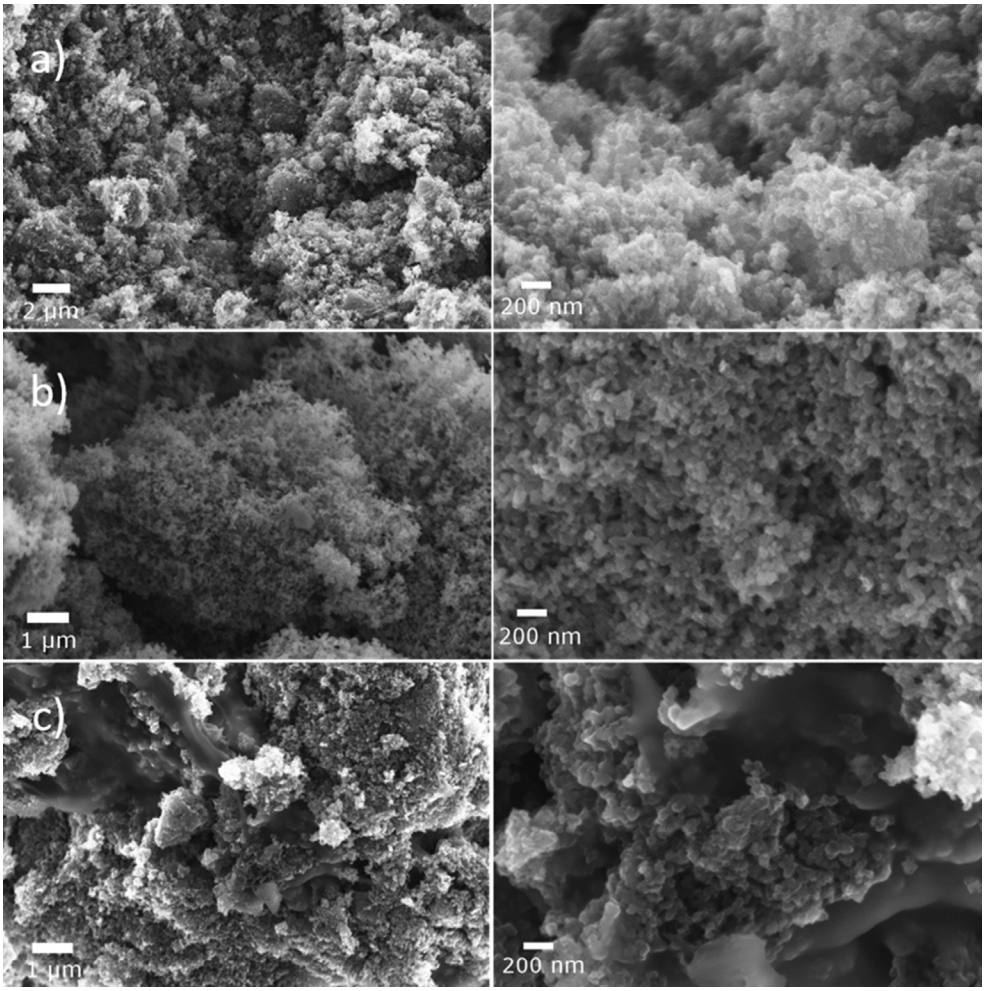

Fig. 2. High resolution SEM images at low resolution (LHS) and high resolution (RHS) of catalyst layer cross section for the cathode with catalyst **FeCo a) I/C 0.5 b) I/C 1 c) I/C 2** (see Supporting Information S10 – S12 for original microscopy images and S13 and S14 for images of catalyst Fe-1 and Fe-2).

catalysts was initially determined by the rotating disk electrode method in 0.5 mol dm^{-3} H_2SO_4 acid at a loading of 750 μg cm^{-2} (Fig. 1a) [29]. This allows comparison of the activity of the catalysts. It is seen that the activity of the **FeCo** catalyst (0.077 A g^{-1} @ 0.8 V vs RHE or 0.192 A cm^{-3} assuming a density of 0.4 g cm^{-2}) [1] is significantly lower than **Fe-1** (0.77 A g^{-1} or 1.93 A cm^{-3}) and **Fe-2** (1.36 A g^{-1} or 3.4 A cm^{-3}) at the same potential. These results demonstrate the differences in the surface area and microstructure, as well as in the activity of the different catalysts.

These materials were fabricated into membrane electrode assemblies (MEA) for single cell performance testing under real operating conditions. The cathode catalyst loading used in this study was 4 mg/cm^2, while the anode loading was 0.4 mg_{Pt}/cm^2 (Alfa Aesar, Johnson Matthey Hydrogen Reformate/Cathode). A relatively high Pt anode loading was chosen in order to ensure that no limiting effects of the anode reaction, which could interfere with the results, were experienced. Fig. 1b shows a representative scanning electron micrograph of the MEA cross section of such a cell. It can be clearly seen that the non-precious metal catalyst layer on the right hand side is significantly thicker (~100 μm) compared to the anode catalyst layer on the left hand side (~10 μm). Such thin catalyst layers as seen in the anode are representative of those seen on the cathode when platinum is used as electrocatalyst. This illustrates the large difference between Pt based and NPMC catalyst layers. This large thickness has a significant impact on properties such as proton and mass transport. It has been shown that the catalyst layer can be represented by a transmission line equivalent circuit, as shown in Fig. 1 c and d [10]. Fig. 1 c shows the transmission line in the absence of a faradaic reaction, i.e. the conditions used where an inert gas such as Argon is supplied to the cathode. Fig. 1 d shows the model in the presence of a faradaic reaction, hence under normal operation.

High resolution SEM images of the catalyst layers of different ionomer content are shown in Fig. 2. It can be clearly seen that ionomer agglomerations are increasingly present for increasing ionomer loading in the sample. It also visualises the structural difference of the 3 investigated catalysts, additional to the difference in BET surface area, microporous and external surface area and BJH pore size distribution.

Electrochemical impedance spectroscopy (*eis*) on single cells operating on H_2/O_2 can be used to extract the high frequency resistance, which is associated with the electronic resistances of the current leads and cell assembly as well as of the membrane. The high frequency resistance corrected cell potential values, Nyquist

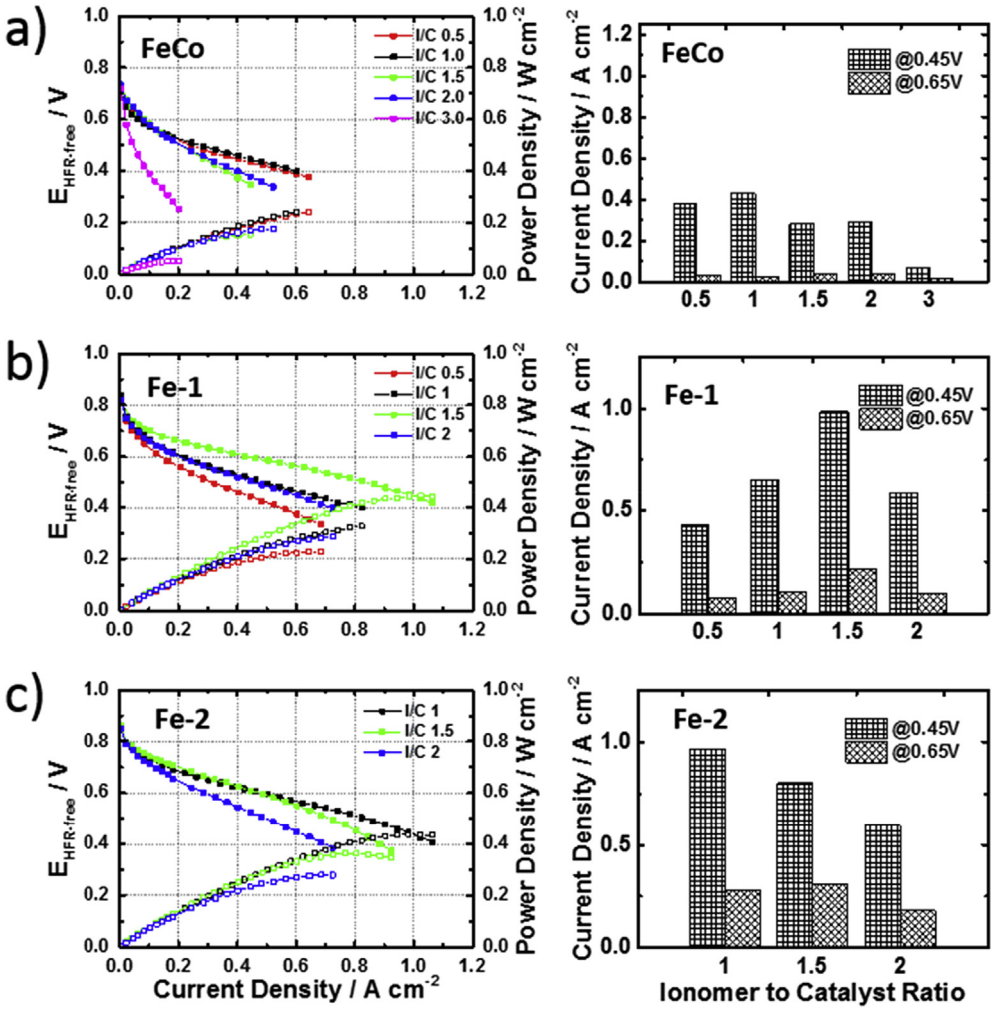

Fig. 3. Left: Galvanostatic polarisation curves for single cells with different ionomer loadings at the cathode, Anode: H_2, 160 sccm, 2 bar back pressure (gauge), 100% RH, Johnson Matthey Hydrogen reformate electrode 0.4 mg_{Pt}/cm^2, Cathode: O_2, 550 sccm, 2 bar back pressure (gauge), 100% RH, $4mg_{catalyst}/cm^2$; Cell Temperature: 80 °C **Right**: Bar plot depicting the respective current density at 2 different cell potentials. **a) FeCo b) Fe-1 c) Fe-2**. Cell voltages are iR corrected using the resistance determined from the high frequency intercept with the real axis in the Nyquist plot.

and Bode plots are better suited to compare catalyst performance, since unrelated performance losses are compensated for. This high frequency corrected cell potential is given by

$$E_{HFR-free} = E_{cell} + j*HFR \quad (1)$$

where $E_{HFR\text{-}free}$ is the high frequency corrected cell potential in V, E_{cell} is the measured uncorrected cell potential in V, j is the current density at the respective cell potential in A cm^{-2} and HFR is the high frequency area specific resistance, as extracted from the real value of the impedance at 0° phase angle in Ω cm^2.

Fig. 3 presents plots of the iR free cell potentials versus current density for the different electrodes, operated with the respective catalysts at different ionomer loadings. Ionomer to catalyst ratios between 0.5 and 3 have been chosen in this study as the optimum value always falls within this range. This is not surprising, given the difference in activity and microstructure. However it is time consuming to determine the optimum ionomer ratio for a specific catalyst. While for the catalysts **FeCo** and **Fe-2** an I/C ratio of 1 has been identified as the optimum, for catalyst **Fe-1** it is 1.5. The current density at 2 different iR corrected cell potentials are depicted in Fig. 3 on the right hand side. It can be seen that at low current densities i.e. high cell potential, the trend is not the same for the catalysts **FeCo** and **Fe-2** which operate better with a low ionomer content at high current densities. For the catalyst **Fe-2**, at low current density, a higher ionomer content is indeed beneficial. The reason might be that with a higher ionomer content more active sites might be accessible. However this benefit might be lost at high current densities, where proton and mass transport become more important.

Further insights into the fuel cell cathode performance can be gained from electrochemical impedance spectroscopy measurements in the absence of a faradaic reaction. Although simple, the transmission line model is suitable to examine H_2/Argon PEMFC single cell properties [6,13,14]. The impedance derived from this transmission line model is given by Ref. [34]:

$$Z(i\omega) = \sqrt{\frac{R_D}{i\omega C_D}}\coth(i\omega R_D C_D) \quad (2)$$

where R_D is the total distributed resistance and C_D the total distributed capacitance. Applying asymptotic approximations one arrives at a 45° line at high frequency and a vertical line towards low frequency in the Nyquist plot [34]. From this feature the proton resistances in catalyst layers have been extracted for Pt based catalysts [6,7,13]. Furthermore one can extract the frequency dispersion in these electrodes which gives rise to the constant phase element (CPE) and is defined as [35].

$$Z_{CPE} = \frac{1}{Q(i\omega)^{\phi}} \quad (3)$$

where, Q is the parameter related to the electrode capacitance (F $s^{\phi-1}$ cm^{-2}), and ϕ is the constant phase exponent and related to the deviation from the pure capacitive line of 90° towards an angle of 90°*ϕ in the Nyquist plot at low frequencies or a deviation of the limiting phase angle below 90° in the Bode phase angle plot [35]. The origin of this CPE can be attributed to adsorption/diffusion processes at the catalyst surface [35]. A CPE behaviour in a fuel cell electrode could therefore originate from inhomogeneous proton diffusion towards the gas diffusion electrode, where the proton mobility is restricted due to low or inhomogeneous ionomer coverage. Hence a higher frequency dispersion might be detrimental for cell performance.

Fig. 4 shows the Nyquist (left, and in expanded view on the right) and Bode phase angle (centre) plots for the cells with the

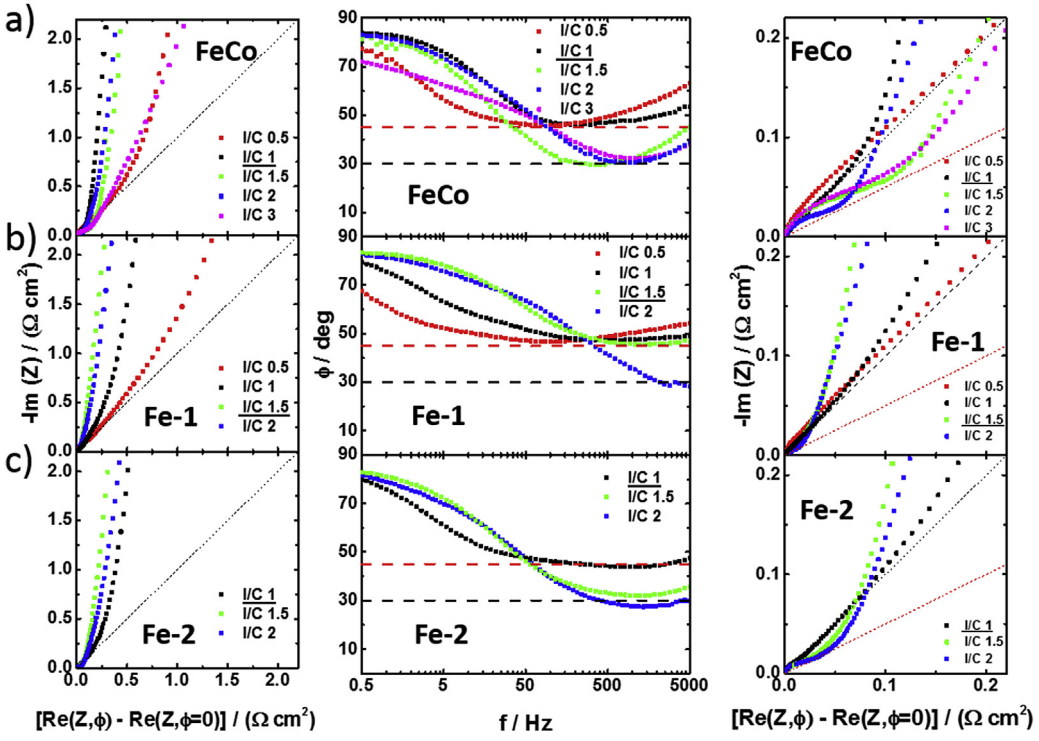

Fig. 4. Left: Nyquist plots, **Centre**: Bode phase angle plots, **Right**: Magnified Nyquist plots, recorded for the cells operating on a) **FeCo** b) **Fe-1** c) **Fe-2** at the cathode at 0.1 V cell potential, Anode: 20 ccm Hydrogen, Cathode: 550 ccm Argon (Bode magnitude plots in Supporting Information). Dashed red line corresponds to 45° in Nyquist plot. Dashed black line corresponds to 30°. (For interpretation of the references to colour in this figure legend, the reader is referred to the web version of this article.)

cathode under an inert environment at 0.1 V with the three different cathode catalysts. Nyquist and Bode plots are corrected for the uncompensated high frequency resistance (uncompensated data can be found in the Supporting Information). Corresponding results for H_2/O_2 single cells under operation are shown in Figs. 5 and 6 for cell potentials of 0.6 V and 0.27 V, respectively.

The results for operation in H_2/Argon (Fig. 4) show that there is a consistent predictor across all three catalysts for the best performing ionomer/carbon ratios. The predictor is based on the phase angle response at low and high frequencies. The best performing systems meet the following criteria:

a) At high frequencies they show phase angles close to 45° (c.f. Eq (2))
b) At low frequencies, they maintain phase angle shifts close to 90° up to the highest possible frequency (c.f. Eq (3))

Moreover, there are two aspects of the phase angle shift which can be used to ascertain whether a catalyst layer has too much or too little ionomer in it:

a) Catalyst layers with too much ionomer show phase shifts below 45°, and tend to approach shifts of 30° (e.g. I/C 1.5,2 and 3 for catalyst FeCo, I/C 2 for Fe-1 and I/C 1.5 and 2 for Fe-2 all show phase angle minima of 30° and contain more ionomer than the optimum value)
b) Catalyst layers with too little ionomer deviate from the low frequency 90° plateau at much lower frequencies than catalyst layers with excess ionomer (e.g. I/C 0.5 for FeCo, I/C 0.5 and 1 for Fe-1).

Hence cells with the highest performance are those which remain close to the 45° phase shift at the highest frequency (red dashed lines in plots) and which show an extended plateau region of ca. 90° in the low frequency Bode phase angle plot. We rationalise this criteria thus: If the electrode is fully flooded with ionomer then the entire porous structure is accessible with the lowest possible pore resistance, and so the system shows an extended low frequency region in which the response is dominated by the electrode capacitance. In our case all electrodes seem to asymptotically approach a limiting phase angle of 85° at low frequency suggesting the constant phase exponent, φ, is close to one. As the ionomer content is decreased, this gives rise to an increasing pore resistance and decreasing coverage of the ionomer on the carbon shifting the phase angle response from ~85° to lower values at a given frequency (i.e. the pole in the frequency response shifts down in

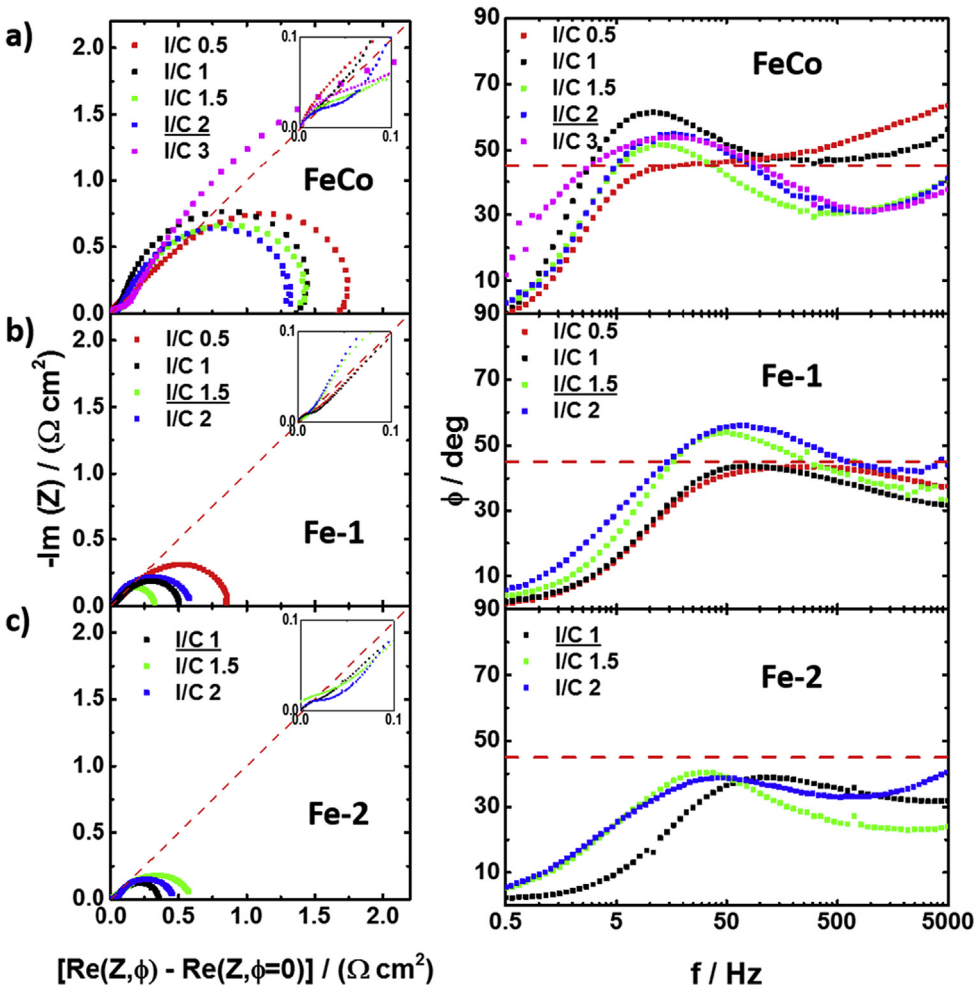

Fig. 5. Left: Nyquist plots, **inset**: magnification of high frequency region **Right**: Bode phase angle plots, recorded for the cells operating on **a) FeCo b) Fe-1 c) Fe-2** at the cathode at 0.6 V cell potential, Anode: 160 sccm Hydrogen, Cathode: 550 sccm Oxygen (Bode magnitude plots in Supporting Information). Dashed red line corresponds to 45° in Nyquist plot. (For interpretation of the references to colour in this figure legend, the reader is referred to the web version of this article.)

frequency). Increasing the ionomer content above the minimum required to suitably access the entire surface area of the catalyst will result in extra transport losses to no benefit of the catalyst performance. The response at high frequency is rationalised on the basis of Eq (2) [34], which predicts a 45° angle line in the phase plot at high frequency [13]. It is interesting that the poorly performing electrodes (i.e. those with too much ionomer) show high frequency phase angles which fall below this value and seem to approach a characteristic value of 30°.

This anomalous effect in the Nyquist plot can also be seen in the fuel cells operating with oxygen on the cathode (Fig. 5, left), especially for the **FeCo** catalyst. Interestingly, this behaviour seems to be correlated with the performance of the iR-corrected results, especially at higher current densities, depicted in Fig. 3.

Another interesting finding is that at high current densities, a significant Warburg impedance is visible in the impedance spectrum (Fig. 6), for the MEAs operating with the better performing catalysts **Fe-1** and **Fe-2**.

This is deduced because of the clearly visible 45° line or indication of a second arc at low frequencies (Fig. 6 b and c left), especially for catalyst **Fe-1** at its optimal I/C ratio of 1.5 and the catalyst **Fe-2** at its optimal I/C ratio of 1. This means that a significant mass transport resistance is present even at a relatively low current density of 1.2 A cm^{-2}. Usually single cells with a similar active area working with Pt based cathode catalyst under pure oxygen can reach current densities that are up to 3–5 times higher before experiencing mass transport limitations [36]. This indicates that not only proton conductivity and catalytic activity have to be optimised, but also the gas transport properties of the catalyst layer have to be taken into account, in order to eventually reach performances similar to Pt based cathodes. Furthermore it can be seen that the maximum in the phase angle (Figs. 5 and 6 right) of the Bode phase plots in the cells operating under H_2/O_2 shifts to lower frequencies at a higher ionomer loading. This is more pronounced under higher current densities, and might indicate that the dispersion of time constants of individual *R*–C elements within the catalyst layer is increasing [35]. In all cases the compositions with the maximum performance are those with the smallest absolute magnitude at low frequencies.

To confirm whether the deviation from the 45° slope, as seen in Fig. 4, can be solely attributed to the ionomer content and is not related to catalyst layer thickness, electrodes with a different loading and hence different thickness were prepared, while using the optimal ionomer content as determined before. Fig. 7a shows the corresponding H_2/Argon single cell Nyquist impedance plot. It can be seen that the slope at high frequency follows the 45° slope without any dependence on the thickness. To rule out any effect of the back pressure, spectra with and without backpressure were

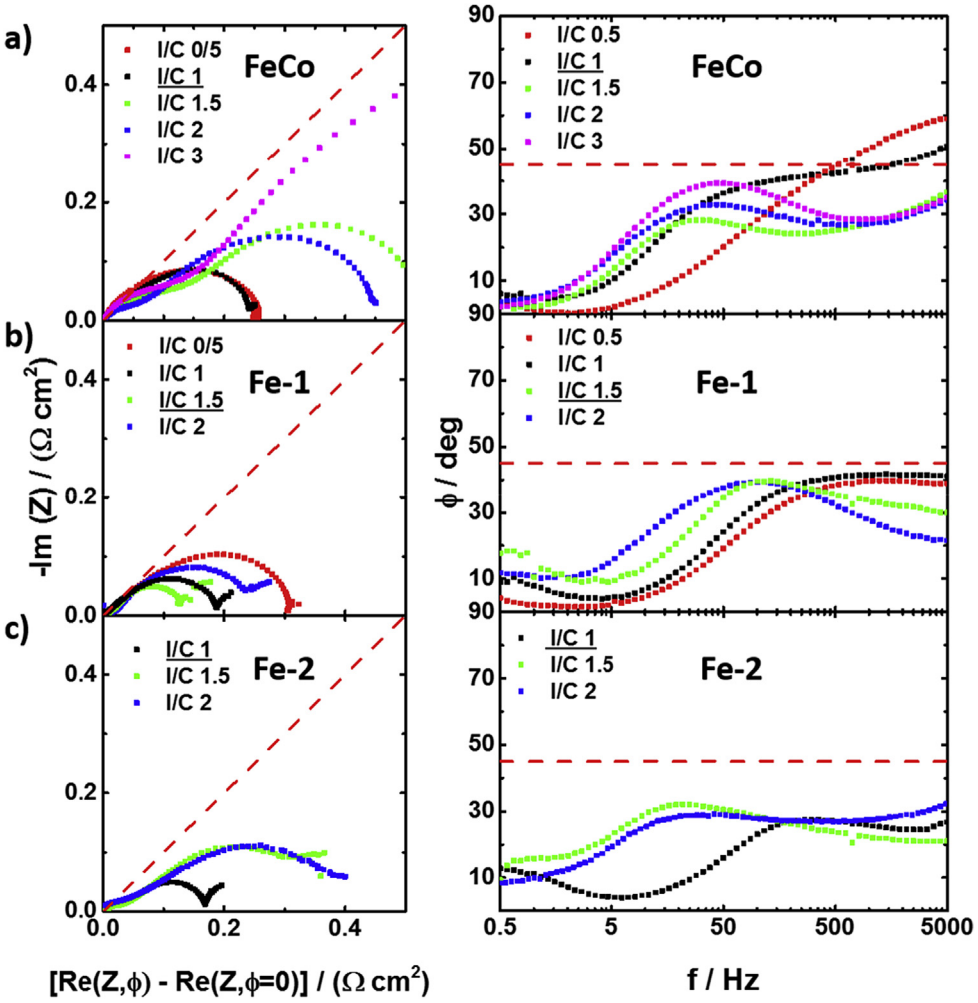

Fig. 6. Left: Nyquist plots **Right**: Bode phase angle plots, recorded for the cells operating on **a) FeCo b) Fe-1 c) Fe-2** at the cathode at 0.27 V cell potential, Anode: 160 sccm Hydrogen, Cathode: 550 sccm Oxygen (Bode magnitude plots in Supporting Information).

recorded (Supporting Information), and these did not evidence a significant effect. These results clearly show that this phenomenon can be solely attributed to processes related to the ionomer. Furthermore, the fact that this effect is present in the absence of a Faradaic reaction means that it is likely correlated with the proton conductivity. To investigate whether this is a structural feature of the electrode or dependent on the operating conditions, the relative humidity and thus the proton conductivity was varied (Fig. 7b,(c)). For a lower RH value, as expected the proton resistance increases.

However for the system with the optimum I/C ratio (Fig. 7b), the 45° slope was retained at all humidities. This indicates that the operating conditions do not exhibit an influence that affects this high frequency feature at the optimal ionomer loading. However a more profound effect is seen for a non-optimised I/C ratio, Fig. 7c. In this case there is a significant variation in the high frequency response with a range of different limiting phase angles seen in the Bode plot.

The impedance study of porous electrodes is a well-developed topic, as it has tremendous practical importance [20,34,35,37–47]. The deviation from 45° at high frequency observed here has been ascribed to different effects. For example, Keiser et al. modelled the impedance response for pores with different shapes [41]. The model is based on a recursive method where the disc is divided into segments with fixed height and radius. Each pore has its own electrolyte resistance and double layer capacitance. The electrolyte resistance down the pore varies according to the respective cross section in this segment. Therefore pores of different shapes can be constructed. The standardized pore impedance is then obtained by a recursion formula. More details are given in Refs. 32 and 35. This means that for the pore with a narrow neck and wide body, the resistance decreases, as the A/C current penetrates deeper into the pore and the cross section has a larger radius. The situation is different for the narrowing pore,

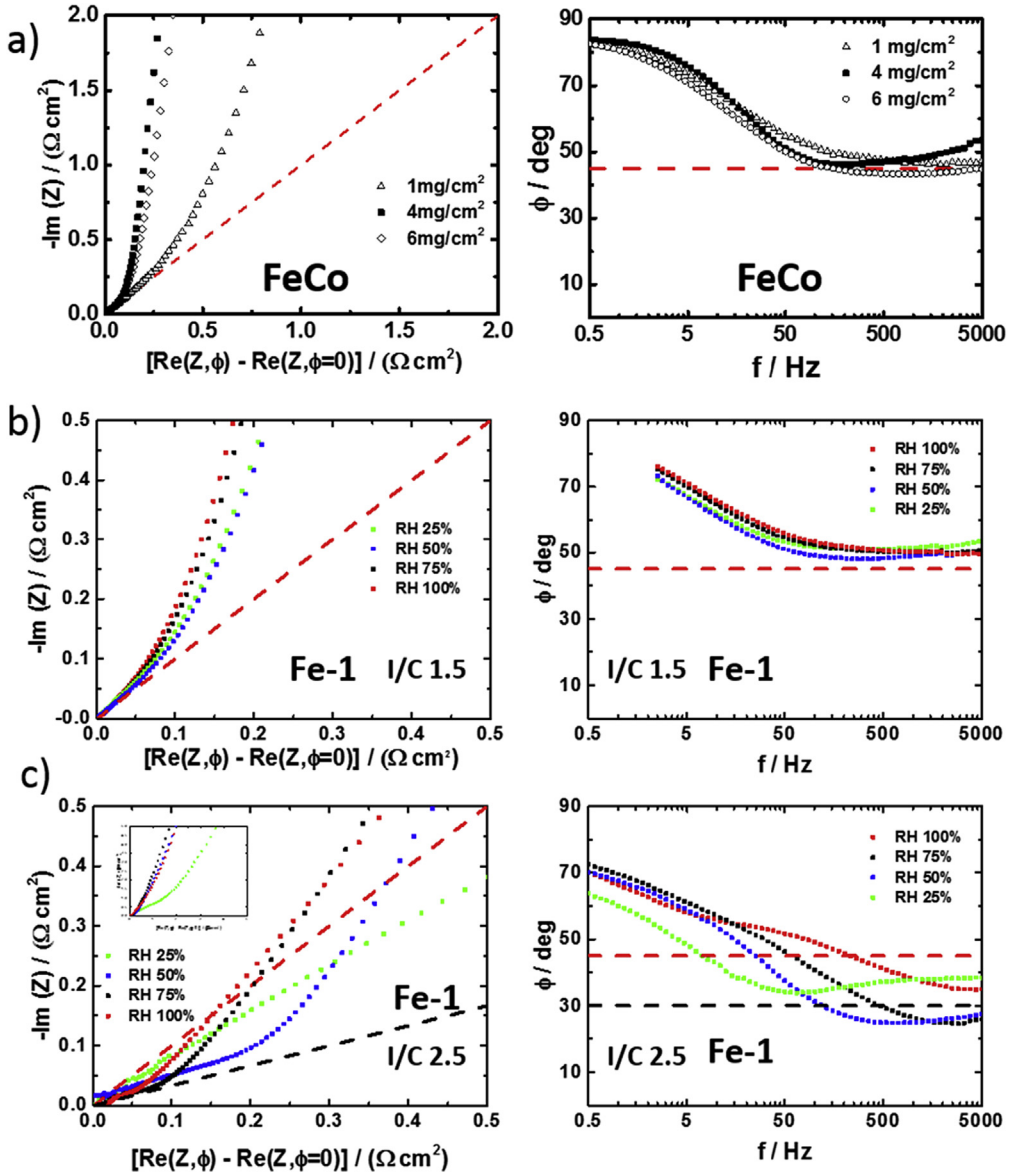

Fig. 7. a) Nyquist plots **(left)** and Bode phase plot (right) for the cells operating on catalyst **FeCo** at the cathode at 0.1 V cell potential with different loadings, Anode: 160 ccm Hydrogen, Cathode: 550 ccm Argon. Dashed red line corresponds to 45° angle. **b)** Nyquist plots for the cell operating on catalyst **Fe-1** for an optimum I/C ratio (a), and a non-ideal ratio (b). 0.1 V cell potential at different relative humidity levels, Anode: 160 ccm Hydrogen, Cathode: 550 ccm Argon. Dashed red line corresponds to 45° angle. (For interpretation of the references to colour in this figure legend, the reader is referred to the web version of this article.)

which has an increasing resistance. In summary, it is found that pore shapes which significantly deviate from a cylindrical geometry lead to a behaviour in the Nyquist plot which is intriguingly similar to that observed in our spectra. This model predicts that when a pore has a narrow mouth and a wide body, the slope drops significantly below the typical 45°, while having a wide pore mouth and narrowing down towards the end of the pore provides a line that stays above 45° as observed for our spectra with low ionomer content. The slope calculated for the perfect cylindrical pore yields the 45° high frequency slope.

These findings have been used to suggest an explanation for the behaviour observed in our spectra. Fig. 8a depicts a model of the carbon particles covered with ionomer. Depending on the ionomer loading different scenarios of pore filling are possible. A too low ionomer loading can lead to pores that are not homogenously covered. The ionomer thickness down the pore would be decreasing as shown in Fig. 8b (left) and the active sites within this pore would not be fully ionically accessible. This would reduce the catalyst utilisation and hence the performance of the electrode. It is assumed that the ionic conductivity of the structure is correlated with the thickness of the ionomer coverage. This can be done as the absolute resistance of an electrolyte (in this case Nafion) is inversely proportional to the area the current of ions is moving through. This means going further down the pore, the cross sectional area of Nafion in the pore decreases and the ionic resistance increases. This is analogous to having a completely electrolyte filled pore which narrows down, thus reducing the electrolyte cross sectional area and increasing the resistance (Fig. 8b middle). The corresponding impedance response which has a phase angle greater than 45° according to the model by Keiser et al. is depicted in Fig. 8b (right). A homogeneous coverage depicted in Fig. 8c (left) will lead to a homogeneous layer thickness and will hence show a uniform resistance down the pore, which is analogous to a cylindrical electrolyte filled pore with a constant diameter (Fig. 8c middle). This will then produce an impedance response with a 45° phase angle (Fig. 8c right). The homogeneous coverage makes all active sites accessible, while only creating a thin barrier for gas transport through the Nafion film, leading to full utilisation and optimal performance. A high ionomer loading as depicted in Fig. 8d (left) will fill up the pore and will lead to a lower resistance further inside the pore where the ionomer thickness is significantly higher. This would translate into a pore with a narrow mouth and wide body (Fig. 8d middle). A phase angle below 45° is then obtained (Fig. 8d right). While in this configuration, all active sites should be ionically accessible, the thick Nafion layer will severely impede gas transport and lead to poor performance. Although this might be an oversimplified model it can explain the anomalous effects observed here and suggests that homogeneous current distribution within the catalyst layer is crucial.

Table 2 correlates the different catalyst I/C ratios with the operating conditions and the performance. It is clear that the best performing I/C ratio for each catalyst always exhibits the desired impedance response. Namely a 45° high frequency phase angle and a close to 90° low frequency phase angle.

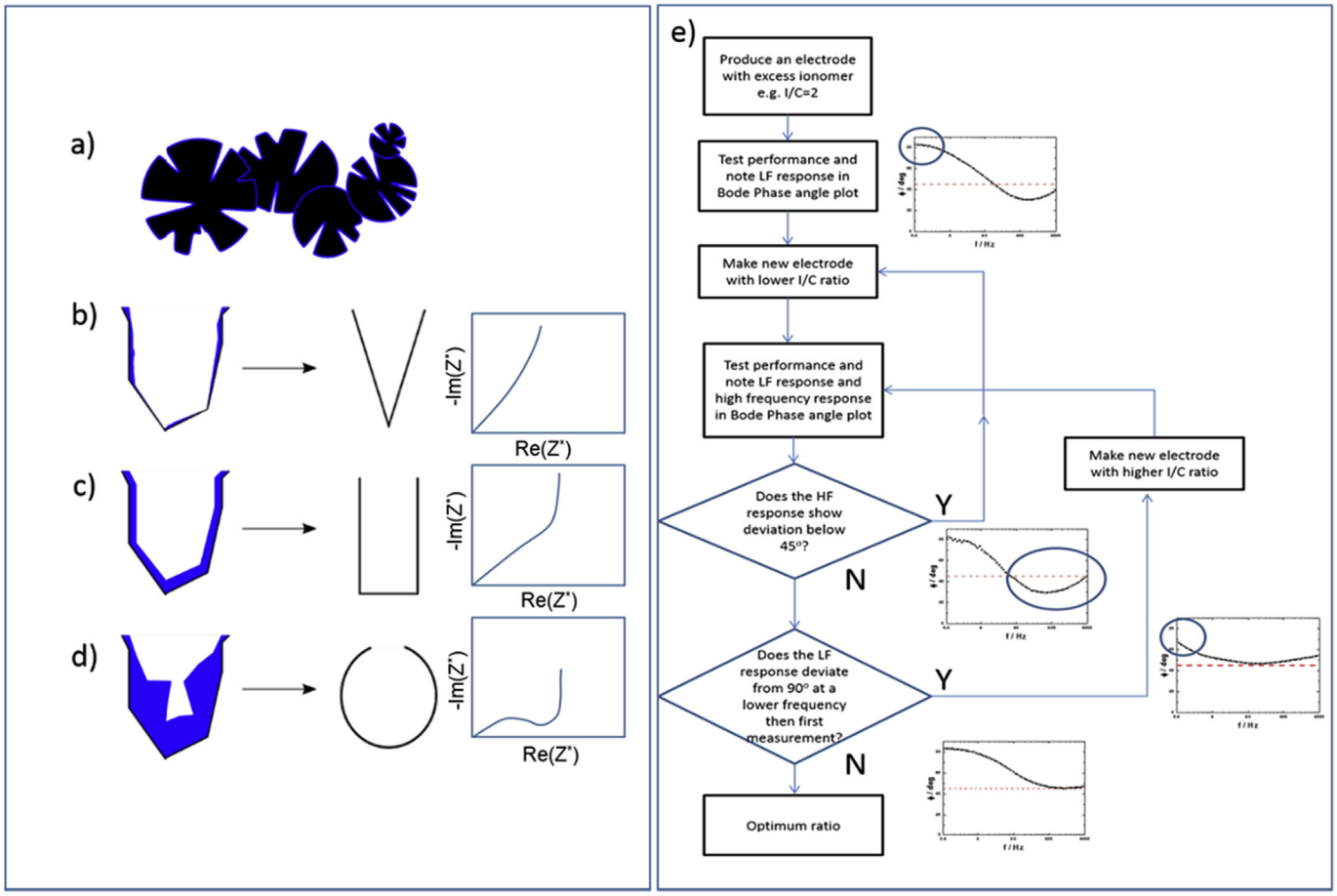

Fig. 8. a) Schematic describing porous carbon covered with a layer of ionomer **b) - d)** showing how the ionomer coverage corresponds to electrolyte filled pores. **b)** incomplete coverage **c)** homogeneous coverage **d)** high loading with inhomogeneously filled pore. On the right hand side are representative Nyquist plots associated with the characteristic pore shapes (taken from ref 33 and 30) **e)** Flow chart illustrating the optimisation strategy to obtain the best performing catalyst layer.

Table 2
Values of the different catalyst I/C ratios and the corresponding H_2/O_2 performance. It can be seen in Fig. 4 that the phase angle under H_2/O_2 which is obtained for the respective I/C ratio under operation conditions as shown in Fig. 3, resembles the phase angle described in Fig. 8.

Ionomer loading (shape of expected Nyquist response is shown in Fig. 8)	Catalyst	I/C ratio	Current density @0.45$V_{iR\text{-}free}$ (under H2/O2 as shown in Fig. 3)
Too low (Fig. 8b)	FeCo	0.5	0.38
	Fe-1	0.5	0.43
	Fe-1	1	0.65
Optimum (Fig. 8c)	FeCo	1	0.43
	Fe-1	1.5	0.98
	Fe-2	1	0.96
Too high (Fig. 8d)	FeCo	1.5	0.28
	FeCo	2	0.29
	FeCo	3	0.067
	Fe-1	2	0.59
	Fe-2	1.5	0.80
	Fe-2	2	0.60

A non-optimal ionomer loading will inevitably lead to an inhomogeneous resistance within the catalyst layer, consistent with the anomalous impedance behaviour observed for the H_2/Argon single cells at high frequencies and the Warburg impedance seen at high current densities for the H_2/O_2 cells. The method proposed here can easily identify the presence of such inhomogeneities and hence significantly aid in strategies for the optimisation of the electrode catalyst layer structures.

In Fig. 8e we provide a simple flow diagram showing how an optimisation process for these electrodes would be implemented. The approach involves making a succession of electrodes and determining their EIS performance in a fuel cell configuration running on H_2/Argon. Utilising this approach we would determine the optimum configuration for all our catalyst systems in a minimum number of steps.

4. Conclusion

By performing an extensive Electrochemical Impedance Spectroscopy (EIS) investigation of three different non-precious metal catalysts with different ionomer content in PEM single cells, it was found that impedance spectroscopy can be used as a diagnostic tool to find an optimised ionomer loading for a given new catalyst. An ionomer coverage which is too high will lead to a deviation from the high frequency 45° line in the Nyquist plot with a tendency to follow a 30° line when the cell is operated in the absence of a Faradaic reaction. Although the suggestion for the source of this phenomenon relies on an oversimplified method it may give an idea of what impact an inhomogenous resistance within pores can exhibit. A flow chart illustrates the steps needed to optimise the catalyst layer and determine the optimum ionomer content. This study will help to speed up the time consuming optimisation of MEAs operated on newly developed catalysts.

Acknowledgements

The Imperial College London Global Engagements Award is greatly acknowledged for providing funds that enabled the international collaboration, along with the Engineering and Physical Sciences (EPSRC) grant EP/J016454/1. Authors also would like to thank CNPq (proc. 150249/2014-4) and FAPESP (proc. 2013/16930-7) for financial assistances.

Appendix A. Supplementary data

Supplementary data related to this article can be found at http://dx.doi.org/10.1016/j.jpowsour.2016.05.035. The data used to generate the plots in this paper are available at http://dx.doi.org/10.5281/zenodo.51438.

References

[1] H.A. Gasteiger, S.S. Kocha, B. Sompalli, F.T. Wagner, Appl. Catal. B Environ. 56 (2005) 9–35.
[2] F. Jaouen, Heat-treated transition metal-NxCy electrocatalysts for the O2 reduction reaction in acid PEM fuel cells, in: Z. Chen, J.-P. Dodelet, J.Z. Dodelet (Eds.), Non-Noble Metal Fuel Cell Catalysts, Wiley-VCH Verlag GmbH & Co. KGaA, 2014, pp. 29–118.
[3] F. Jaouen, E. Proietti, M. Lefèvre, R. Chenitz, J.-P. Dodelet, G. Wu, H.T. Chung, C.M. Johnston, P. Zelenay, Energy Environ. Sci. 4 (2010) 114–130.
[4] in, 2013.
[5] F. Jaouen, V. Goellner, M. Lefèvre, J. Herranz, E. Proietti, J.P. Dodelet, Electrochimica Acta 87 (2013) 619–628.
[6] Y. Liu, C. Ji, W. Gu, D.R. Baker, J. Jorne, H.A. Gasteiger, J. Electrochem. Soc. 157 (2010) B1154–B1162.
[7] K.C. Neyerlin, W. Gu, J. Jorne, H.A. Gasteiger, J. Electrochem. Soc. 153 (2006) A1955–A1963.
[8] J.-P. Dodelet, The controversial role of the metal in Fe- or Co-Based electrocatalysts for the oxygen reduction reaction in acid medium, in: M. Shao (Ed.), Electrocatalysis in Fuel Cells, Springer, London, 2013, pp. 271–338.
[9] M. Eikerling, A.A. Kornyshev, J. Electroanal. Chem. 453 (1998) 89–106.
[10] M. Eikerling, A.A. Kornyshev, J. Electroanal. Chem. 475 (1999) 107–123.
[11] H. Iden, K. Sato, A. Ohma, K. Shinohara, J. Electrochem. Soc. 158 (2011) B987–B994.
[12] M.C. Lefebvre, R.B. Martin, P.G. Pickup, Electrochem. Solid State Lett. 2 (1999) 259–261.
[13] Y. Liu, M. Murphy, D. Baker, W. Gu, C. Ji, J. Jorne, H.A. Gasteiger, ECS Trans. 11 (2007) 473–484.
[14] R. Makharia, M.F. Mathias, D.R. Baker, J. Electrochem. Soc. 152 (2005) A970–A977.
[15] D. Malevich, B.R. Jayasankar, E. Halliop, J.G. Pharoah, B.A. Peppley, K. Karan, J. Electrochem. Soc. 159 (2012) F888–F895.
[16] D.R.P. Morris, S.P. Liu, D. Villegas Gonzalez, J.T. Gostick, ACS Appl. Mater. Interfaces 6 (2014) 18609–18618.
[17] E. Passalacqua, F. Lufrano, G. Squadrito, A. Patti, L. Giorgi, Electrochimica Acta 46 (2001) 799–805.
[18] R. Roshandel, F. Ahmadi, Renew. Energy 50 (2013) 921–931.
[19] A.P. Saab, F.H. Garzon, T.A. Zawodzinski, J. Electrochem. Soc. 149 (2002) A1541–A1546.
[20] J.S. Yi, T.-w. Song, J. Electrochem. Soc. 160 (2013) F141–F152.
[21] S. Stariha, K. Artyushkova, A. Serov, P. Atanassov, Int. J. Hydrogen Energy 40 (2015) 14676–14682.
[22] E. Proietti, F. Jaouen, M. Lefèvre, N. Larouche, J. Tian, J. Herranz, J.-P. Dodelet, Nat. Commun. 2 (2011) 416.
[23] Y. Nabae, Y. Kuang, M. Chokai, T. Ichihara, A. Isoda, T. Hayakawa, T. Aoki, J. Mater. Chem. A 2 (2014) 11561–11564.
[24] G. Wu, K.L. More, C.M. Johnston, P. Zelenay, Science 332 (2011) 443–447.
[25] J. Shui, C. Chen, L. Grabstanowicz, D. Zhao, D.-J. Liu, Proc. Natl. Acad. Sci. 112 (2015) 10629–10634.
[26] K. Strickland, E. Miner, Q. Jia, U. Tylus, N. Ramaswamy, W. Liang, M.-T. Sougrati, F. Jaouen, S. Mukerjee, Nat. Commun. 6 (2015) 7343.
[27] J.-Y. Choi, R.S. Hsu, Z. Chen, J. Phys. Chem. C 114 (2010) 8048–8053.
[28] D. Malko, T. Lopes, E. Symianakis, A.R. Kucernak, J. Mater. Chem. A 4 (2015) 142–152.
[29] U.A. Paulus, T.J. Schmidt, H.A. Gasteiger, R.J. Behm, J. Electroanal. Chem. 495 (2001) 134–145.
[30] V.A. Paganin, E.A. Ticianelli, E.R. Gonzalez, J. Appl. Electrochem. 26 (1996) 297–304.
[31] B.A. Boukamp, J. Electrochem. Soc. 142 (1995) 1885–1894.
[32] M. Schönleber, E. Ivers-Tiffée, Electrochem. Commun. 58 (2015) 15–19.

[33] M. Schönleber, D. Klotz, E. Ivers-Tiffée, Electrochimica Acta 131 (2014) 20–27.
[34] I.D. Raistrick, Electrochimica Acta 35 (1990) 1579–1586.
[35] E.M. Davis, C.M. Stafford, K.A. Page, ACS Macro Lett. 3 (2014) 1029–1035.
[36] T.E. Springer, T.A. Zawodzinski, M.S. Wilson, S. Gottesfeld, J. Electrochem. Soc. 143 (1996) 587–599.
[37] J. Bisquert, G. Garcia-Belmonte, F. Fabregat-Santiago, A. Compte, Electrochem. Commun. 1 (1999) 429–435.
[38] K. Eloot, F. Debuyck, M. Moors, A.P.V. Peteghem, J. Appl. Electrochem. 25 (1995) 326–333.
[39] R.d.P.B. Hernández, I.V. Aoki, B. Tribollet, H.G. de Melo, Electrochimica Acta 56 (2011) 2801–2814.
[40] C. Hitz, A. Lasia, J. Electroanal. Chem. 500 (2001) 213–222.
[41] H. Keiser, K.D. Beccu, M.A. Gutjahr, Electrochimica Acta 21 (1976) 539–543.
[42] A. Lasia, J. Electroanal. Chem. 500 (2001) 30–35.
[43] M. Musiani, M. Orazem, B. Tribollet, V. Vivier, Electrochimica Acta 56 (2011) 8014–8022.
[44] G. Paasch, K. Micka, P. Gersdorf, Electrochimica Acta 38 (1993) 2653–2662.
[45] H.-K. Song, H.-Y. Hwang, K.-H. Lee, L.H. Dao, Electrochimica Acta 45 (2000) 2241–2257.
[46] Wiley: Impedance Spectroscopy: Theory, Experiment, and Applications, second ed. - Evgenij Barsoukov, J. Ross Macdonald.
[47] J.R. Park, D.D. Macdonald, Corros. Sci. 23 (1983) 295–315.